JOC The Journal of Organic Chemistry

Article

pubs.acs.org/joc

Alternative Route Toward Nitrones: Experimental and Theoretical Findings

Damir A. Safin,*[,†] Mariusz P. Mitoraj,*[,‡] Maria G. Babashkina,[†] Piotr Kubisiak,[‡] Koen Robeyns,[†] and Yaroslav Filinchuk[†]

[†]Institute of Condensed Matter and Nanosciences, Molecules, Solids and Reactivity (IMCN/MOST), Université catholique de Louvain, Place L. Pasteur 1, 1348 Louvain-la-Neuve, Belgium

[‡]Department of Theoretical Chemistry, Faculty of Chemistry, Jagiellonian University, R. Ingardena 3, 30-060 Cracow, Poland

Supporting Information

ABSTRACT: Nitrones are important building blocks for natural and biologically active compounds, used as spin-trap reagents and therapeutic agents. All this makes nitrones intriguing and valuable compounds for fundamental studies and as useful chemicals in various synthetic strategies. Therefore, nitrones are still of great interest and in the limelight of researches. With our initial goal to solve synthetic problems toward 5-phenyl-2,2′-bipyridine (**Phbpy**), we found that this reaction can proceed through the formation of 6-phenyl-3-(pyridin-2-yl)-1,2,4-triazin-4(3H)-ol (**4-OH**), which rapidly isomerizes to a 3,4-dihydro-1,2,4-triazine-based nitrone, namely 6-phenyl-3-pyridin-2-yl-2,3-dihydro-1,2,4-triazin-4-oxide (**4′**), This encouraged us to study condensation of hydrazonophenylacetaldehyde oxime (**2**), obtained from 2-isonitrosoacetophenone (**1**), with other aldehydes. The reaction with both salicylaldehyde and *p*-tolualdehyde leads to the open-chain isomers, namely (2-hydroxybenzylidene)hydrazono-2-phenylacetaldehyde oxime (**5**) and (4-methylbenzylidene)hydrazono-2-phenylacetaldehyde oxime (**6**), respectively. The latter product exists in solution in equilibrium with its cyclic isomer 6-phenyl-3-(4-methylphenyl)-2,3-dihydro-1,2,4-triazin-4-oxide (**6′**), while the former one exists in solution exclusively in the open-chain form. It was also found that **2** reacts with acetone with the formation of 3,3-dimethyl-6-phenyl-2,3-dihydro-1,2,4-triazin-4-oxide (**7′**), which also exists in solution in equilibrium with its open-chain isomer 2-phenyl-2-(propan-2-ylidenehydrazono)acetaldehyde oxime (**7**). The static DFT as well as ab initio molecular dynamics simulations have corroborated the experimental findings.

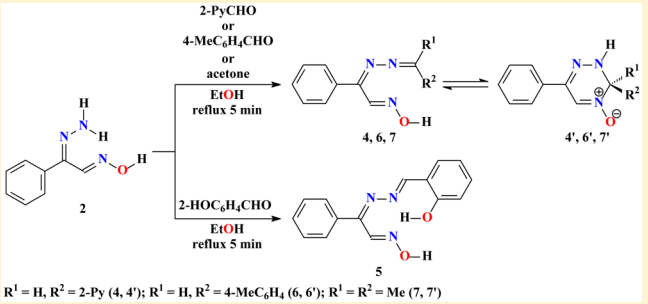

INTRODUCTION

A nitrone, $R^1R^2C{=}N^+(O^-)R^3$ ($R^3 \neq H$), is a functional group in organic chemistry, and an *N*-oxide of an imine (Scheme 1, A). Depending on the degree of substitution at the carbon atom, aldonitrones (R^1 = H, R^2—an organic radical) and ketonitrones (R^1, $R^2 \neq H$) are distinguished. Nitrones are easily prepared by several well-developed methods. The most widely used includes condensation reactions between carbonyl compounds[1,2] and oxidation of amines, imines, or hydroxylamines.[3,4] Since nitrones were first discovered more than a century ago,[5,6] their chemistry has been well explored.[7−9] Nitrones are important building blocks for natural and biologically active compounds,[10−12] used as spin-trap reagents[13−16] and therapeutic agents.[17−19]

The electronic structure of the nitrone group, except for the main structure A, includes three canonical structures B−D (Scheme 1).[20] Their relative contributions are determined by internal structural characteristics of the nitrones and by the influence of external factors, such as polarity of the solvent, of hydrogen bond formation, complexation, and protonation. Changes in the electronic structure of nitrones can be qualitatively explained by analyzing the relative contribution of A−D structures. However, it has been established that the C−N bond in nitrones is almost of a pure double bond nature, while that between the N and O atoms is of a partial double bond nature.[21,22] Neither experimental nor computational data have, however, been reported for the structures C and D.

Scheme 1

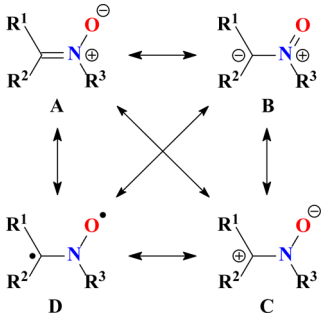

Received: November 25, 2016
Published: January 17, 2017

DOI: 10.1021/acs.joc.6b02821
J. Org. Chem. 2017, 82, 1666−1675

Scheme 2

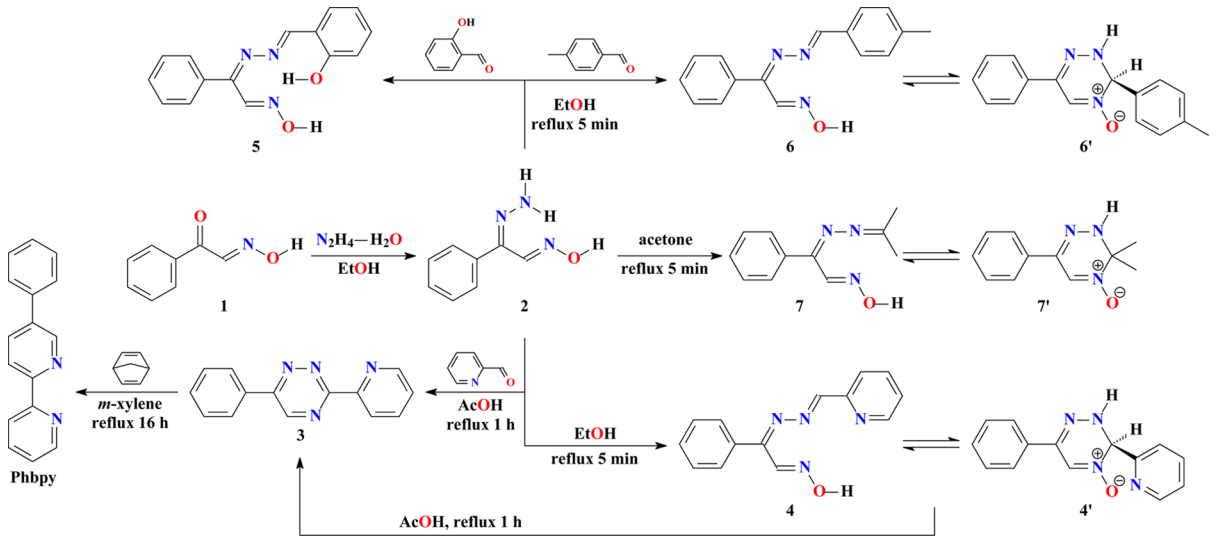

Nitrones are intriguing and valuable compounds for fundamental studies and useful building blocks in various synthetic strategies.[20,23−29] Thus, nitrones are still of great interest and in the limelight of researches due to their diversity in chemical properties and synthetic utility.

We have recently directed our attention to the 5-phenyl-2,2′-bipyridine (**Phbpy**).[30] Although an efficient synthesis of this ligand from 2-isonitrosoacetophenone (**1**) was described,[31,32] we were faced with a number of problems during isolation of its precursors, namely hydrazonophenylacetaldehyde oxime (**2**) and 6-phenyl-3-(pyridin-2-yl)-1,2,4-triazine (**3**). This, probably, explains the lack of metal complexes of both **2** and **3** as well as general unavailability of **Phbpy**.

With our initial goal to solve synthetic problems toward **Phbpy**, we, surprisingly, found for the first time that this reaction can proceed through the formation of 6-phenyl-3-(pyridin-2-yl)-1,2,4-triazin-4(3*H*)-ol (**4-OH**),[31,33] which rapidly isomerizes to a 3,4-dihydro-1,2,4-triazine-based nitrone, namely 6-phenyl-3-pyridin-2-yl-2,3-dihydro-1,2,4-triazin-4-oxide (**4′**), which exists in solution in equilibrium with its open-chain isomer (pyridin-2-ylmethylene)hydrazono-2-phenylacetaldehyde oxime (**4**). This intriguing finding encouraged us to study condensation of **2** with other aldehydes, namely salicylaldehyde and *p*-tolualdehyde, and acetone.

In this work, we describe the novel protocol on synthesis and facile isolation of **2**, **3**, and **Phbpy** as well as the formation of 3,4-dihydro-1,2,4-triazine-based nitrones. The equilibrium between nitrone structures and their corresponding open-chain isomers was determined and studied for the first time by ^{1}H NMR spectroscopy. Theoretical static DFT and ab initio dynamics investigations were also performed in order to elucidate a mechanism of nitrone ↔ oxime isomerization as well as to shed light on differences in the electronic structure between the synthesized nitrones and the corresponding open chain isomers.

RESULTS AND DISCUSSION

The oxime **2** was synthesized by reacting 2-isonitrosoacetophenone, **1**, with hydrazine hydrate in ethanol (Scheme 2). It is important to note that the as-synthesized resulting oil was extracted with Et_2O to separate the desired product from viscous dark brown oil. This allowed us to simplify further procedures and to obtain large X-ray suitable crystals of **2**, while skipping of extraction with Et_2O leads to a contamination with an oily residue and complicates crystallization. The ^{1}H NMR spectrum of **2** in $CDCl_3$ exhibits a single set of signals (Figure S1 in the Supporting Information). The signals for the phenyl protons were observed at 7.27−7.56 ppm, while the NH_2, CNH, and OH protons were shown at 8.00, 8.26, and 8.44 ppm, respectively.

The oxime **2** was further involved in the reaction with 2-pyridinecarboxaldehyde in glacial acetic acid, and as a result the doubly substituted 1,2,4-triazine **3** was isolated (Scheme 2). The ^{1}H NMR spectrum of **3** in $CDCl_3$ (Figure S2 in the Supporting Information) contains two multiplets for the phenyl protons at 7.55−7.63 and 8.15−8.23 ppm, while a singlet peak for the triazine proton was shown at 9.19 ppm. The pyridine protons were found in the spectrum as four peaks with different multiplicity at 7.48, 7.94, 8.74, and 8.89 ppm.

Using ethanol instead of glacial acetic acid leads to the products of monocondensation upon reacting **2** with 2-pyridinecarboxaldehyde, salicylaldehyde, or *p*-tolualdehyde, respectively (Scheme 2). Surprisingly, while condensation with the latter two aldehydes leads to the formation of open-chain Schiff bases **5** and **6**, respectively, the same reaction with the former aldehyde yielded a 3,4-dihydro-1,2,4-triazine-based nitrone **4′**.

Interestingly, it was found that the oxime **2** readily reacts with acetone yielding another 3,4-dihydro-1,2,4-triazine-based nitrone **7′** (Scheme 2).

The ^{1}H NMR spectrum of **5** in $CDCl_3$ (Figure S4 in the Supporting Information) contains a single set of signals testifying to the exclusive existence of an open-chain isomer in solution. However, the ^{1}H NMR spectra of **4′** and **6** in $CDCl_3$, and **7′** in DMSO-d_6 (Figures S3, S5, and S6 in the Supporting Information) each reveal two sets of signals corresponding to the nitrone (**4′**, **6′**, and **7′**), and open-chain (**4**, **6**, and **7**) isomers, respectively (Scheme 2). While the ratio between these two isomers is about 1:1 for the compound **6**, 6.25:1 and 10:1 ratios in favor of the nitrone structure were found in the spectra of **4′** and **7′**.

The crystal structures of **2**, **3**, **4′**, **5**, **6**, and **7′** were elucidated by single crystal X-ray diffraction. Compounds **2**, **4′**, **6**, and **7′** crystallize in the monoclinic space groups $P2_1/n$, Pn, $P2_1/c$, and

DOI: 10.1021/acs.joc.6b02821
J. Org. Chem. 2017, 82, 1666−1675

$P2_1$, respectively, while the structures of compounds **3** and **5** were refined in the orthorhombic space groups $Pca2_1$ and $Pna2_1$, respectively.

The N−N═C−C═N−O fragment of the molecule of **2** is almost planar (Figure 1, Figure S7 and Table S1 in the Supporting Information), which is retained due to an intramolecular hydrogen bond of the N−H···N(O)═C type (Table S7 in the Supporting Information). The dihedral angle between the least-squares planes formed by the N−N═C−C═N−O fragment and the phenyl ring in the crystal structure is about 32°, making the global shape of the molecule of **2** appear nonplanar (Figure 1). The crystal structure of **2** is further stabilized by bifurcated intermolecular hydrogen bonds of the O−H···N−N type (Figure 1, Table S7 in the Supporting Information). As a result of these intermolecular hydrogen bonds, molecules of **2** form 1D polymeric chains of a herringbone-like structure (Figure 1), which, in turn, are linked in 2D sheets through intermolecular hydrogen bonds of the N−H···N−N-type (Figure 1, Table S7 in the Supporting Information).

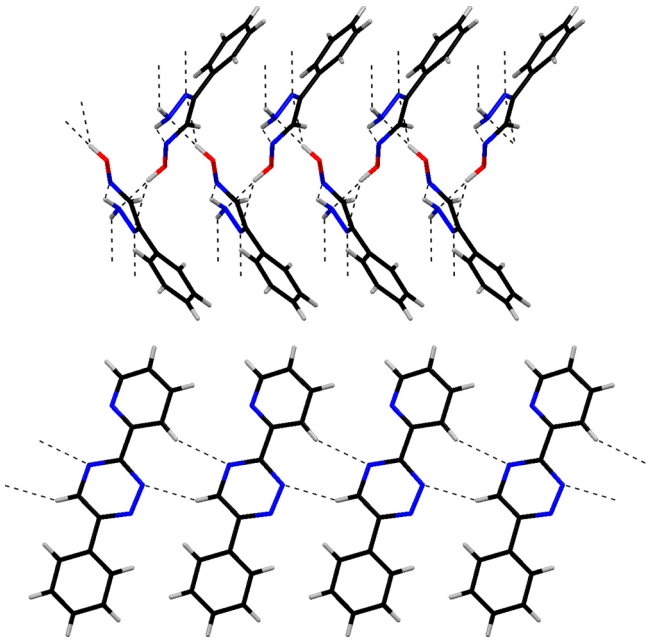

Figure 1. View on the hydrogen bonded 1D chain in the structure of **2** (top) and 1D ribbon in the structure of **3** (bottom). Color code: C = black, H = light gray, N = blue, O = red.

Refinement of the crystal structure of compound **3** was a great challenge. Several plate-like crystals were tested, all diffracting poorly, the current data set diffracting the furthest. Although data were collected up to 0.83 Å a data cutoff of 0.95 Å was imposed during integration,[34] beyond which the data (based on I/s and the R_{int}) were too poor. The structure was initially solved in the space group *Pn*, with six independent molecules in the asymmetric unit. Although the structural outline of the molecules was clear from the structure solution, the assignment of the atom types was not straightforward, especially since a similar ligand **Phbpy** was previously found to be statistically disordered.[30] Discrimination of the atom type based on temperature factors was not always possible and final atom type assignment was complemented by monitoring the unfavorable short inter- and intra- H···H interactions. Molecules of **3** are packed side by side (Figure 1) with potential short intermolecular contacts, which were flagged as undesirable if shorter than the sum of the van der Waals radii minus 0.25 Å. In the final structure no such contacts are observed. Moreover, four nonclassical hydrogen bonds of the C−H···N-type are observed (Table S7 in the Supporting Information), which stabilize 1D ribbons of **3** (Figure 1). After transformation to the noncentrosymmetric space group $Pca2_1$ the three remaining molecules in the asymmetric unit of the crystal structure of **3** were found to display off-centered parallel displaced $\pi\cdots\pi$ stacking with an interplanar separation of about 3.6 Å.

According to the X-ray data, the 3,4-dihydro-1,2,4-triazine ring in **7′** adopts a screw-boat ($<\theta> \sim 65°$, $<\phi> \sim 277°$)[35] conformation (Figure 2 and Figure S12 in the Supporting Information). The central ring in **4′** is less confined to a particular conformation and is found between an envelope conformation and a screw-boat conformation (Figure 2 and Figure S9 in the Supporting Information) with for both structures the tetrahedral carbon showing the maximum out-of-plane deviation from the least-squares plane through the triazine ring (Figure 2, Table S3 and S6 in the Supporting Information).

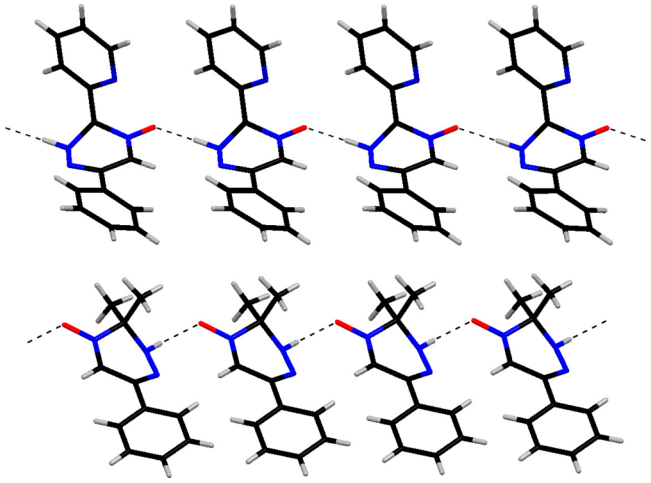

Figure 2. View on the hydrogen bonded 1D chain in the structures of **4′** (top) and **7′** (bottom). Color code: C = black, H = light gray, N = blue, O = red.

Furthermore, this plane also includes the oxygen atom (Figure 2). No structures with a similar central ring can be found in the CSD database, a wider search to establish target values for the nitrone C═N double bond and the N^+-O^- bond results in values of 1.303(19) Å and 1.299(20) Å, respectively. The average C═N bond lengths for **4′** (1.31 Å) and **7′** (1.29 Å) as well as the N^+-O^- bond lengths (1.31 Å for **4′** and 1.29 Å for **7′**) are in line with the retrieved values. As comparison, target values for N−OH were found to be 1.381(14) Å, excluding the possibility of a hydroxylamine isomer. The structures of both **4′** and **7′** are stabilized by intermolecular hydrogen bonds of the N−H···O−N-type (Figure 2, Table S7 in the Supporting Information).

Molecules of **5** and **6** are isomorphic (Figure 3, Figures S10 and S11 in the Supporting Information) and both correspond to Schiff bases. Overall the molecules of **5** and **6** are flat (Figure 3, Table S4 and S5 in the Supporting Information), with the phenyl rings significantly rotated (about 62 and 47° in **5** and **6**, respectively) out of the plane. The molecule of **5** was found in

DOI: 10.1021/acs.joc.6b02821
J. Org. Chem. 2017, 82, 1666−1675

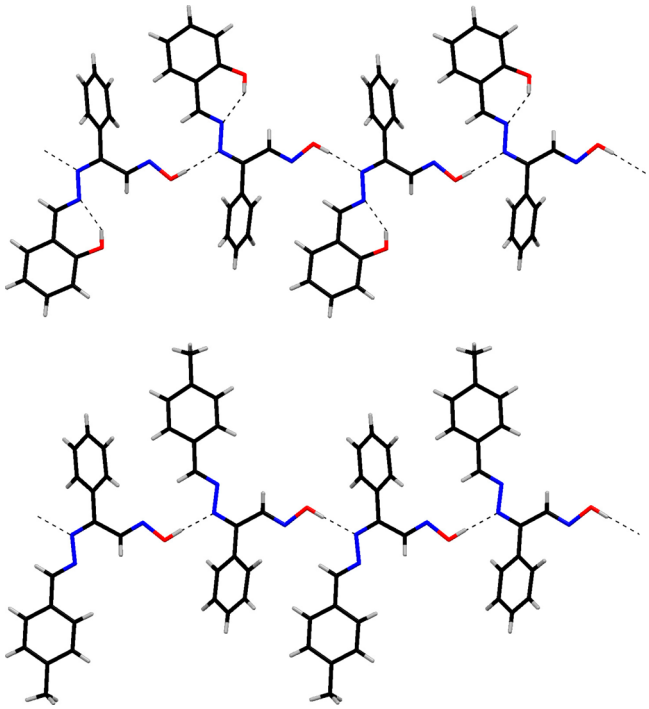

Figure 3. View on the hydrogen bonded 1D chain in the structures of **5** (top) and **6** (bottom). Color code: C = black, H = light gray, N = blue, O = red.

the enolimine form with respect to the 2-OHC_6H_4CHN fragment (Figure 3). The bond length of C−O is about 1.34 Å and that of 2-OHC_6H_4−CH is about 1.45 Å, which indicates single bonds, whereas a double bond of about 1.29 Å is revealed for 2-OHC_6H_4CH═N (Table S4 in the Supporting Information). The crystal structure of **5** exhibits an intramolecular hydrogen bond of the O−H···N-type (Figure 3, Table S7 in the Supporting Information). The structures of both **5** and **6** are stabilized by intramolecular hydrogen bonds of the O−H···N-type (Figure 3, Table S7 in the Supporting Information).

In order to study in details intermolecular interactions in the crystal structures of **1**−**3**, **4′**, **5**, **6**, and **7′**, a Hirshfeld surface analysis has been applied[36] together with the charge and energy decomposition based (ETS-NOCV) analyses and the obtained data are discussed in the Supporting Information.

In order to shed additional light on the equilibrium for the studied complexes we have at first stage performed static DFT calculations at the 6-31G**/6-311++G** levels of theory with the BLYP functional including the empirical correction (D3) for dispersion interactions by Grimme et al.[37] as implemented in the Gaussian 09 rev. D01 package.[38] For each of the considered structure we have considered various isomers (rotamers) based on the relaxed potential energy surface scans. The typical energy profile for **5′** is shown in Figure S13 in the Supporting Information. After the lowest energy conformation was found, its geometry was re-optimized in the larger basis set (6-311++G**). The lowest free energy structures of each species are depicted in Figure 4.

As far as relative stabilities are concerned, the open chain isomer **5** is exclusively populated, while for the remaining molecules the nitrone and open-chain isomers are in equilibrium (Table 1). These findings are in agreement with the experimental NMR data. Considering solvent effects at the PCM level does not change the qualitative conclusion and reveals the open chain isomer **5** is still exclusively present in solution, while both the nitrone and open chain forms are populated for the remaining systems (Table 1). In particular, domination of the nitrone isomers **4′** and **7′** over the corresponding open chain forms **4** and **7**, respectively, is in agreement with the NMR experiments (Table 1). Our calculations based on PCM/BLYP-D3/6-311++G**, however, suggest that the open chain isomer **6** is superior to the nitrone form **6′**, while the ratio of 1:1 was observed in the experimental NMR data. It is important to note that the difference in relative energies by ∼1 kcal/mol, which is the chemical accuracy of quantum chemical calculations, results in a very significant variation in population (∼30%). Furthermore, the accuracy of DFT computations can be often worse than 1 kcal/mol. This means that any type of approximation used in calculations (e.g., continuum approximation of a solvent) can affect final energies and consequently lead to the observed inconsistency.

Nevertheless, the equilibrium between **6** and **6′** is evidently noted, which is in agreement with the experimental data (Table 1). Notably, the suggested in the literature[31,33] alcoholic type isomers, referred here as **4-OH**, **5-OH**, **6-OH**, and **7-OH** (Figure 4), appeared to be significantly higher in energy by about 14−24 kcal/mol (Table 1) compared with the corresponding nitrone and open chain forms.

We have further found that significant stability of the open chain isomer **5**, resulting in the exclusive population of this form, can originate from the existence of the strong intramolecular hydrogen bond O−H···N as suggested by the reduced density gradient surfaces plotted within the non covalent index (NCI) method (Figure 5).[39,40] It should be noted, that contours describing the reduced density gradient for **5** are obtained and discussed in the light of the open chain preference in solution and therefore must be rather related to the isolated molecule. This explains that some minor contribution from the weak intramolecular hydrogen bond C−H···N is also observed (Figure 5). The latter interaction is, however, absent in the crystal structure of **5** since this nitrogen atom is involved in the stronger intermolecular hydrogen bond with the H−O(N) hydrogen atom of a neighboring molecule (Figure 3). It is important to note that O−H···N interaction is also present during the molecular dynamics simulations at T = 298 K (see the Supporting Information video). A similar stability of the nitrone and open chain isomers for the remaining systems might be related to the π-system delocalization resulting in the presence of partially double C−C and C−N bonds as evidenced from the calculated bond-orders by means of the Nalewajski−Mrozek approach (Figure S14 in the Supporting Information).[41] It has been proven that such indices provide very reliable results due to both applying differential density as well inclusion of ionic and covalent contributions, as opposed to other purely density-based techniques.[41]

Furthermore, we have performed on the example of **4′** in-depth analyses of a charge distribution in the nitrone isomers based on molecular electrostatic potential as well as atomic charges (Figure S15 in the Supporting Information). The negative charge is observed at the oxygen atom of the N−O group, whereas the positive partial charges are noted for the remaining atoms in the vicinity of the nitrone unit. Similar is valid for the remaining nitrone isomers. As far as the corresponding open chain isomers are concerned, surprisingly, the nucleophilic area is noted at the entire N−O fragment

DOI: 10.1021/acs.joc.6b02821
J. Org. Chem. 2017, 82, 1666−1675

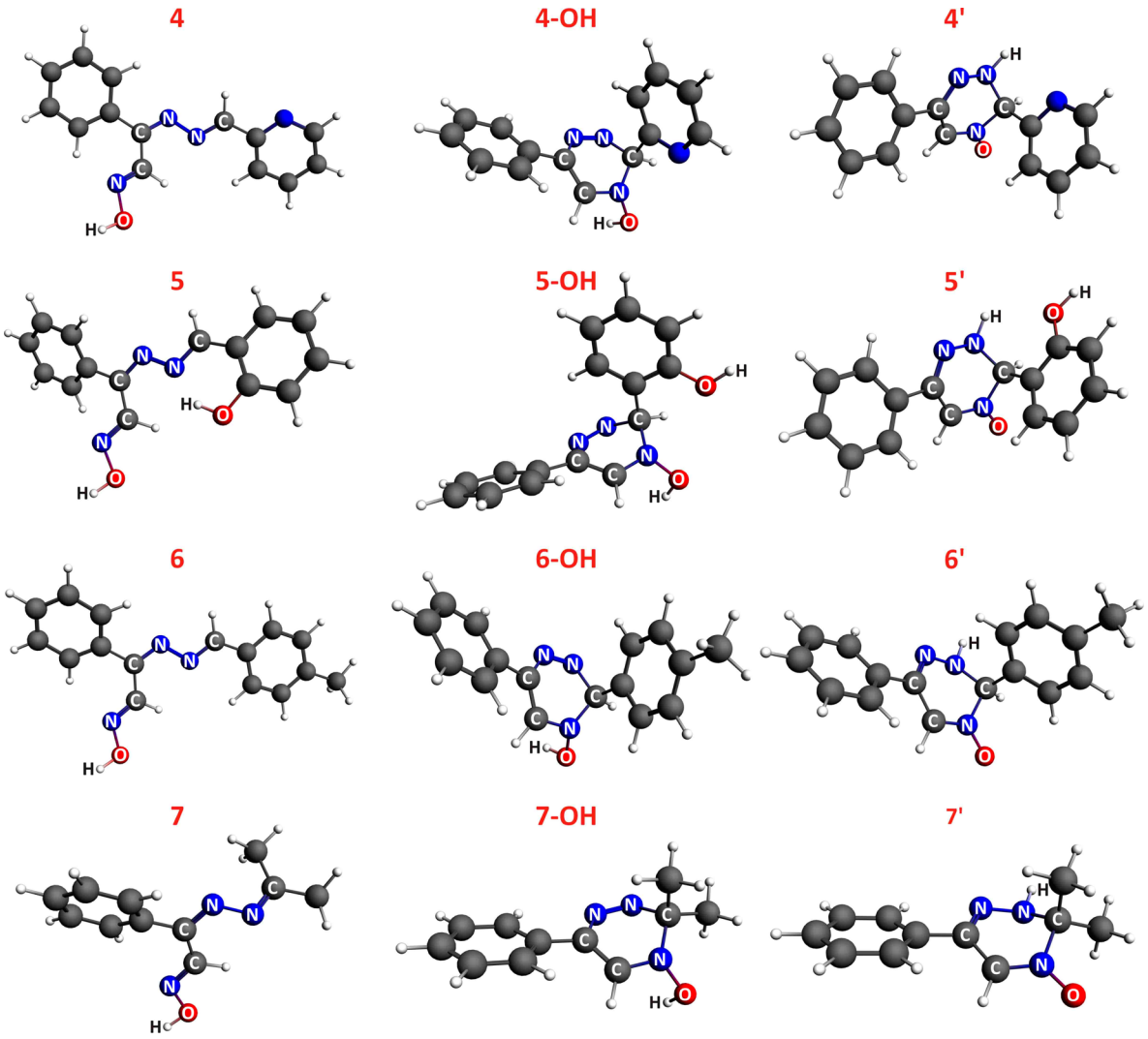

Figure 4. Optimized isomers for different species of **4′**, **5**, **6**, and **7′** obtained from the BLYP-D3/6-311++G** calculations.

Table 1. Relative Free Energies of the Studied Isomers from BLYP-D3/6-311++G Calculations Performed in the Gas Phase (VAC) and in Solvent (PCM), and the Resulting Populations Found According to the Boltzmann Distribution Law**

	VAC		PCM	
structure	ΔG (kcal/mol)	population (%)	ΔG (kcal/mol)	population (%)
4	0.1	45.8	1.3	9.8
4-OH	14.2	0.0	14.1	0.0
4′	0.0	54.2	0.0	90.2
5	0.0	100.0	0.0	100.0
5-OH	23.3	0.0	20.7	0.0
5′	9.0	0.0	7.0	0.0
6	1.8	4.7	1.5	7.5
6-OH	14.5	0.0	15.1	0.0
6′	0.0	95.3	0.0	92.5
7	0.0	70.6	3.5	0.3
7-OH	14.3	0.0	16.0	0.0
7′	0.5	29.4	0.0	99.7

(Figure S16 in the Supporting Information). Such differences in electrophilic/nucleophilic character of the N−O fragment in

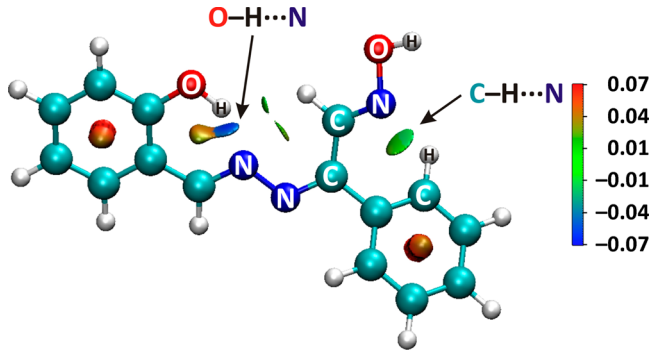

Figure 5. Contours describing the reduced density gradient at the isovalue of 0.5 au for **5**. The surfaces are colored in a blue-green-red scale according to the values of sign($\lambda 2$)ρ, ranging from −0.07 to 0.07 au.

the nitrone and open chain forms might result in diverse reactivity. We have tried to correlate these theoretical results, based on the calculated bond orders and charge distributions, with the intuitive concept of resonance structures (Scheme 1). It is seen that the calculated bond orders of the NO and adjacent CN bonds are 1.61 and 1.48, respectively, indicating their partial double bond character (Figure S15 in the

DOI: 10.1021/acs.joc.6b02821
J. Org. Chem. 2017, 82, 1666−1675

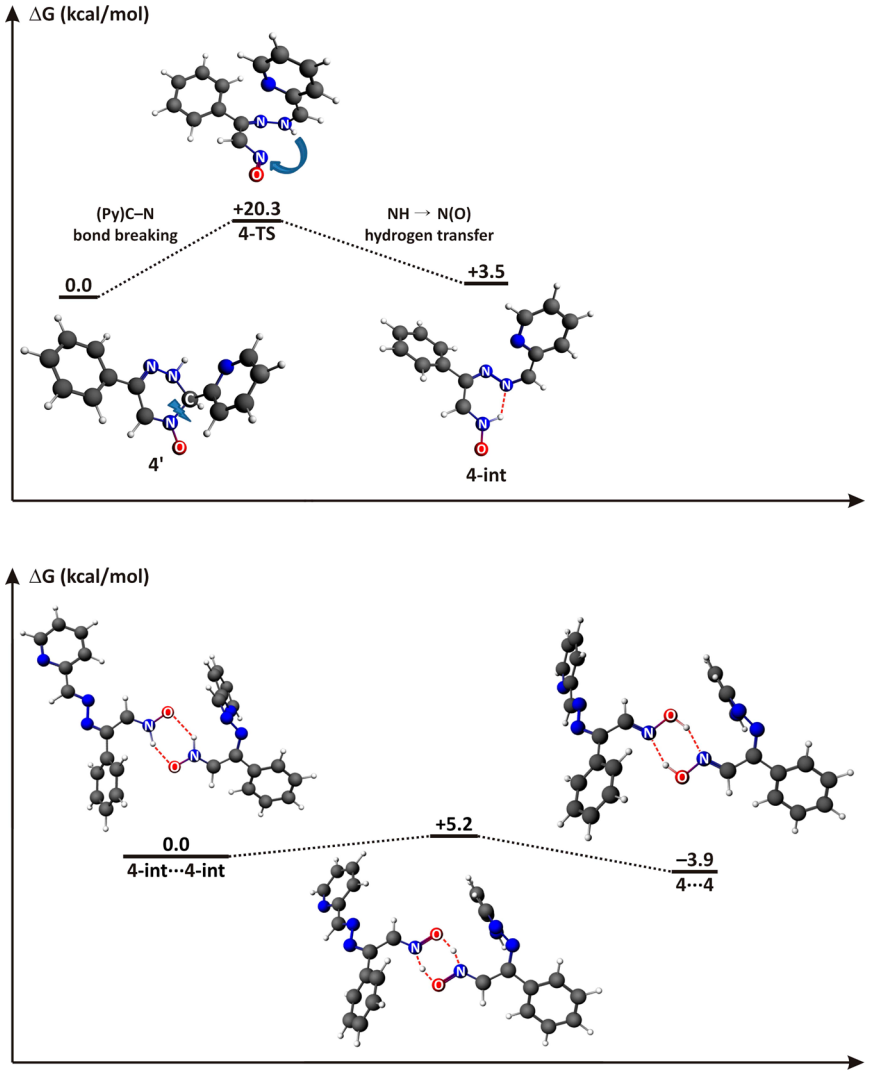

Figure 6. Calculated free energy (ΔG) profile, obtained from the ADF/COSMO/DFT/BLYP-D3/TZP calculations, describing the isomerization mechanism from **4′** to **4**, involving the formation of a hydrogen bonded dimeric species.

Supporting Information). This demonstrates, together with molecular electrostatic potentials, that the nitrone isomers are better described as the combination of the resonance structures A and C (Figure S15 in the Supporting Information).

At the next stage, a possible mechanism of isomerization between the nitrone form **4′** and its open chain isomer **4** was modeled. Various mechanisms were considered (Figure S17–S19 in the Supporting Information). We have determined that at the first stage the (Py)C–N bond of **4′** is broken followed by spontaneous hydrogen atom transfer NH → NO. This leads to the formation of the stable nitrone intermediate **4-int** (Figure 6, top). This step is characterized by a relatively low kinetic barrier (ΔG = +20.3 kcal/mol). We have also performed constraint molecular dynamics simulations[42−44] of **4′** by gradual elongation of the (Py)C–N bond. It was found, similarly to the static DFT calculations, a spontaneous hydrogen transfer NH → NO yielding **4-int** (see the Supporting Information video). We have further found that the typical 1,2-hydrogen shift mechanism starting from **4-int**, leading to the formation of **4**, is not likely to occur due to a very high energy barrier +52 kcal/mol (Figure S17 in the Supporting Information). The stepwise mechanism, where the diazine hydrogen atom in **4′** migrates first to the carbon atom, followed by the H-transfer to the oxygen atom (Figure S18 in the Supporting Information), was also excluded. We have also declined a possibility where the (Py)C–N bond of **4′** is broken at the first stage followed by the hydrogen transfer NH → NO (Figure S19 in the Supporting Information). Therefore, we have inferred that a further process starting from **4-int** can proceed intermolecularly. In particular, **4-int** can easily dimerize via two N–H···O hydrogen bonds due to a stabilizing, by −13.4 kcal/mol (BLYP-D3/TZP), intermolecular interaction (Figure 6, bottom). We have also confirmed the stability of the **4-int**···**4-int** dimer by the molecular dynamics simulations (see the Supporting Information video). On the next stage the facile tautomerization of **4-int**···**4-int** occurs due to a small kinetic barrier giving rise to the formation of the open chain hydrogen bonded adduct **4**···**4** (Figure 6, bottom).

It should be noted, that the mechanism of oxime-nitrone tautomerism has been revisited by Roca-López and co-workers.[45] It has been reported, in line with our mechanistic proposal, that the isomerization is rather of the intermolecular nature as opposed to the intramolecular scenario. Furthermore, the mechanism proposed herein nicely explains why the nitrone isomer is not formed in the case of the open chain isomer **5**. In particular, the nitrogen atom of the hydrazine unit, which is

DOI: 10.1021/acs.joc.6b02821
J. Org. Chem. 2017, 82, 1666−1675

crucial in the overall mechanism as it acts as the hydrogen acceptor, is already blocked by the intramolecular hydrogen bond N···H−O with the phenolic hydroxyl group (Figures 3 and 5). This, in turn, means that the reaction from **4-int** to **4′** cannot proceed (Figure 6). We have also discarded a mechanistic possibility where the dimer of **4′** can be formed via N−H···O hydrogen bonding. Although it exhibits a minimum on the potential energy surface (**4′**···**4′**) at the static DFT level (gas phase, 0 K), it appeared to be unstable (has drifted apart) at a more realistic condition (T = 298 K) as revealed from the molecular dynamics simulations.

We have also characterized the nitrone and open-chain isomers by the Born−Oppenheimer molecular dynamics simulations. It has been found that both **4′** and **4** alone are stable compounds, i.e. during the simulation of both species the lack of any spontaneous molecular reorganization/isomerization is noted (see the Supporting Information videos). It is fully in agreement with very high energy barriers noted for the proposed intramolecular hydrogen atom transfers (Figures S17−S19 in the Supporting Information) as well as with a relatively high barrier of the proposed rate-determining step from **4′** to **4** (Figure 6, top). Similar is valid for the remaining systems.

CONCLUSIONS

In summary, we found that the reaction toward 5-phenyl-2,2′-bipyridine (**Phbpy**) via the triazine **3**, most likely, proceeds through the formation of 6-phenyl-3-(pyridin-2-yl)-1,2,4-triazin-4(3*H*)-ol (**4-OH**), which rapidly isomerizes to a 3,4-dihydro-1,2,4-triazine-based nitrone, namely 6-phenyl-3-pyridin-2-yl-2,3-dihydro-1,2,4-triazin-4-oxide (**4′**). The latter nitrone exists in solution in equilibrium with its open-chain isomer (pyridin-2-ylmethylene)hydrazono-2-phenylacetaldehyde oxime (**4**). This encouraged us to study condensation of hydrazonophenylacetaldehyde oxime (**2**), obtained from 2-isonitrosoacetophenone (**1**), with other aldehydes.

The reaction with both salicylaldehyde and *p*-tolualdehyde leads to the open-chain isomers, namely (2-hydroxybenzylidene)hydrazono-2-phenylacetaldehyde oxime (**5**) and (4-methylbenzylidene)hydrazono-2-phenylacetaldehyde oxime (**6**), respectively. The latter product exists in solution in equilibrium with its cyclic isomer 6-phenyl-3-(4-methylphenyl)-2,3-dihydro-1,2,4-triazin-4-oxide (**6′**), while the former one exists in solution exclusively in the open-chain form. It was also found that **2** reacts with acetone, also leading to the formation of a 3,4-dihydro-1,2,4-triazine-based nitrone, namely 3,3-dimethyl-6-phenyl-2,3-dihydro-1,2,4-triazin-4-oxide (**7′**), which also exists in solution in equilibrium with its open-chain isomer 2-phenyl-2-(propan-2-ylidenehydrazono)-acetaldehyde oxime (**7**).

The observed equilibrium between the nitrone and open-chain isomers has been corroborated by the theoretical DFT static and *ab initio* molecular dynamics simulations. It was found that the isomerization mechanism is based on the breaking of the (Py)C−N bond in nitrone followed by the intermolecular tautomerization. We have also shed light on the stability of the synthesized structures by both the Hirshfeld surface analyses and the results stemming from the charge and energy decomposition calculations.

Finally, we trust that the route toward nitrones discovered by us will significantly impact this intriguing field as well as boost further in-depth studies of the reported compounds with respect to their chemical and physical properties. In particular, the reported here nitrone-open chain equilibrium is obviously a powerful tool to switching, e.g., thermo- and photochromic properties of the properly designed compounds.

EXPERIMENTAL SECTION

Materials and Physical Measurements. Hydrazine hydrate (80%, N_2H_4 51%), 2-pyridinecarboxaldehyde (99%), salicylaldehyde (99%), *p*-tolualdehyde (97%), and 2-isonitrosoacetophenone (97%) were used for syntheses. All solvents were of spectroscopic grade and used without further purification. ^{1}H spectra were obtained on a 500 MHz spectrometer at 25 °C and were recorded at 500.13300 MHz. Chemical shifts are reported with reference to $SiMe_4$.

DFT Calculations. We have performed the DFT calculations based on the BLYP-D3/6-311++G** as implemented in the Gaussian 09 rev. D01 package[38] as well as by the ADF suit of programs[46,47] (considering the BLYP-D3/TZP). The PCM solvent model as implemented in the Gaussian 09 program was applied. The COSMO/ADF was also used for mechanistic investigations.

Non-Covalent Index (NCI) Technique. It has been shown that the reduced density gradient, $s = \frac{1}{2(3\pi^2)^{1/3}}\frac{|\nabla\rho|}{\rho^{4/3}}$, appeared to be a useful quantity[39,40] for the description of noncovalent interactions. In order to obtain information about the type of bonding, plots of the reduced density gradient s vs molecular density ρ is examined. When a weak inter- or intramolecular interaction is present, a characteristic spike, lying at low values of both density ρ and reduced density gradient s, exists. To distinguish between attractive and repulsive interactions, the eigenvalues (λi) of the second derivative of density (Hessian, $\nabla^2\rho$) are used, $\nabla^2\rho = \lambda1 + \lambda2 + \lambda3$. Namely, bonding interactions are characterized by $\lambda2 < 0$, whereas $\lambda2 > 0$ indicates that atoms are in a nonbonded contact. Therefore, within the NCI technique, one can draw information about noncovalent interactions from the plots of sign($\lambda2$)ρ vs s. In such plots the low gradient spike, an indicator of the stabilizing interaction, is located within the region of negative values of density. On the contrary, the repulsive interaction is characterized by positive values of sign($\lambda2$)ρ. The contour of s, colored by the value of sign($\lambda2$)ρ, can also be plotted. This gives a pictorial representation of noncovalent interactions.

CP2K Molecular Dynamics Simulations. Ab initio molecular dynamics simulations were performed with the CP2K 2.4 package.[42−44] The BLYP functional with the dispersion correction of Grimme was used with the DZVP molecularly optimized basis sets. Simulations have considered the NVT ensemble at T = 298 K with the Nose−Hoover thermostat and 0.5 fs time step, collected up to 35 ps of trajectory.

Molecular Electrostatic Potential. The electrostatic potential $V(r)$ of a molecule at the point "r", due to nuclei and electrons, is given by eq 1.

$$V(r) = \sum_{A} \frac{Z_A}{|R_A - r|} - \int \frac{\rho(r')dr'}{|r - r'|} \quad (1)$$

where Z_A is the charge of nucleus at position R_A and $\rho(r)$ is the total electronic density. The sign of $V(r)$ depends upon whether the positive contribution of the nuclei or negative from the electrons is dominant. Negative values of $V(r)$ correspond to nucleophilic areas of a molecule, whereas the positive values to electrophilic regions.

DOI: 10.1021/acs.joc.6b02821
J. Org. Chem. 2017, 82, 1666−1675

Synthesis of 2.[31,32] Hydrazine hydrate (2.0 g) was added dropwise under vigorous stirring to a solution of 2-isonitrosoacetophenone (3.0 g, 20 mmol) in EtOH (10 mL). The mixture was stirred at room temperature for 2 h. The solvent was then removed *in vacuo*. The resulting oil was extracted with Et_2O (3 × 50 mL) and the solvent was then removed *in vacuo*. The oily residue was dissolved in CH_2Cl_2 (60 mL) and *n*-hexane (30 mL) was added to a final yellow solution. Yellowish rod-like X-ray suitable crystals were formed during the next day. Crystals were filtered off, washed with *n*-hexane (3 × 30 mL) and air-dried. Yield: 1.17 g (36%). ^{1}H NMR ($CDCl_3$), δ: 7.27−7.41 (m, 3H, *m*-Ph + *p*-Ph), 7.49−7.56 (m, 2H, *o*-Ph), 8.00 (br. s, 2H, NH_2), 8.26 (s, 1H, CHN), 8.44 (br. s, 1H, OH) ppm. Anal. Calc. for $C_8H_9N_3O$ (163.18) (%): C 58.89, H 5.56 and N 25.75; found: C 58.97, H 5.62 and N 25.67.

Synthesis of 3.[31,32] 2-Pyridinecarboxaldehyde (0.54 g, 5 mmol) was added dropwise under vigorous stirring to a solution of **2** (0.7 g, 4.29 mmol) in glacial acetic acid (10 mL). The mixture was refluxed for 1 h. The solvent was then removed *in vacuo*. The resulting oil was dissolved in hot EtOH (20 mL), left for slow evaporation and crystals were formed during the next day. Crystals were filtered off, washed with Et_2O (3 × 30 mL), and dissolved in a minimum amount of EtOH. Colorless plate-like X-ray suitable crystals were formed during the next day. Crystals were filtered off, washed with Et_2O (3 × 30 mL), and air-dried. Yield: 0.69 g (69%). ^{1}H NMR ($CDCl_3$, peaks were assigned with help of ^{1}H−^{1}H COSY experiments), δ: 7.55−7.63 (m, 3H, *m*-Ph + *p*-Ph), 8.15−8.23 (m, 2H, *o*-Ph), 7.48 (d. d. d, $^3J_{H,H}$ = 7.9 Hz, $^3J_{H,H}$ = 4.7 Hz, $^4J_{H,H}$ = 1.1 Hz, 1H, 4-H, Py), 7.94 (t. d, $^3J_{H,H}$ = 7.9 Hz, $^4J_{H,H}$ = 1.8 Hz, 1H, 5-H, Py), 8.74 (d. t, $^3J_{H,H}$ = 7.9 Hz, $^4J_{H,H}$ = 1.1 Hz, 1H, 6-H, Py), 8.89 (d. d. d, $^3J_{H,H}$ = 4.7 Hz, $^4J_{H,H}$ = 1.8 Hz, $^5J_{H,H}$ = 0.8 Hz, 1H, CHN, Py), 9.19 (s, 1H, triazine) ppm. Anal. Calc. for $C_{14}H_{10}N_4$ (234.26) (%): C 71.78, H 4.30 and N 23.92; found: C 71.66, H 4.38 and N 23.84.

Synthesis of 4′, 5, and 6. 2-Pyridinecarboxaldehyde, salicylaldehyde, or *p*-tolualdehyde (0.54, 0.61, and 0.60 g, respectively; 5 mmol) was added dropwise under vigorous stirring to a solution of **2** (1.0 g, 4.27 mmol) in EtOH (10 mL). The mixture was refluxed for 5 min. The resulting solution was left for slow evaporation and X-ray suitable crystals were formed during the next day. Crystals were filtered off, washed with *n*-hexane (3 × 30 mL), and air-dried.

4′:[31,32]Pale yellow rod like crystals. Yield: 1.06 g (84%). ^{1}H NMR ($CDCl_3$, peaks were assigned with help of ^{1}H−^{1}H COSY experiments), δ: 5.97 (s, 6.25H, CHNN, **4′**), 7.31 (d. d. d, $^3J_{H,H}$ = 7.6 Hz, $^3J_{H,H}$ = 4.8 Hz, $^4J_{H,H}$ = 0.9 Hz, 6.25H, 5-H, Py, **4′**), 7.33−7.46 (m, 22.75H, *m*-Ph + *p*-Ph, **4′** + **4**), 7.53 (d, $^3J_{H,H}$ = 7.8 Hz, 6.25H, 3-H, Py, **4′**), 7.56−7.61 (m, 12.5H, *o*-Ph, **4′**), 7.71 (t. d, $^3J_{H,H}$ = 7.8 Hz, $^4J_{H,H}$ = 1.7 Hz, 6.25H, 4-H, Py, **4′**), 7.75 (br. s, 6.25H, NH, **4′**), 7.80 (t. d. d, $^3J_{H,H}$ = 7.8 Hz, $^4J_{H,H}$ = 1.7 Hz, $^5J_{H,H}$ = 0.6 Hz, 1H, 4-H, Py, **4**), 7.83−7.86 (m, 2H, *o*-Ph, **4**), 7.87 (s, 6.25H, CHNO, **4′**), 8.18 (d. t, $^3J_{H,H}$ = 7.9 Hz, $^4J_{H,H}$ = 1.1 Hz, 1H, 3-H, Py, **4**), 8.56 (s, 1H, CHNOH, **4**), 8.62 (d. d. d, $^3J_{H,H}$ = 4.9 Hz, $^4J_{H,H}$ = 1.7 Hz, $^5J_{H,H}$ = 0.9 Hz, 6.25H, 6-H, Py, **4′**), 8.71 (d. d. d, $^3J_{H,H}$ = 4.9 Hz, $^4J_{H,H}$ = 1.7 Hz, $^5J_{H,H}$ = 0.9 Hz, 1H, 6-H, Py, **4**), 8.94 (s, 1H, CHNN, **4**), 10.39 (br. s, 1H, OH, **4**) ppm. Anal. Calc. for $C_{14}H_{12}N_4O$ (252.28) (%): C 66.65, H 4.79 and N 22.21; found: C 66.79, H 4.72 and N 22.32.

5: Yellow block-like crystals. Yield: 1.31 g (98%). ^{1}H NMR ($CDCl_3$, peaks were assigned with help of ^{1}H−^{1}H COSY experiments), δ: 6.98 (t. d, $^3J_{H,H}$ = 7.4 Hz, $^4J_{H,H}$ = 1.6 Hz, 1H, C_6H_4), 7.05 (d, $^3J_{H,H}$ = 8.5 Hz, 1H, C_6H_4), 7.37 (d. d, $^3J_{H,H}$ = 7.5 Hz, $^4J_{H,H}$ = 1.6 Hz, 1H, C_6H_4), 7.42 (t. d, $^3J_{H,H}$ = 7.4 Hz, $^4J_{H,H}$ = 1.6 Hz, 1H, C_6H_4), 7.44−7.52 (m, 3H, *m*-Ph + *p*-Ph), 7.81 (d, $^4J_{H,H}$ = 1.6 Hz, 1H, *o*-Ph), 7.83 (d, $^4J_{H,H}$ = 1.6 Hz, 1H, *o*-Ph), 8.36 (br. s, 1H, NOH), 8.66 (s, 1H, CHNOH), 8.75 (s, 1H, CHNN), 11.50 (br. s, 1H, OH, C_6H_4OH) ppm. ^{13}C NMR spectrum is not available due to poor solubility. Anal. Calc. for $C_{15}H_{13}N_3O_2$ (267.29) (%): C 67.41, H 4.90 and N 15.72; found: C 67.54, H 4.84 and N 15.81.

6: Yellow block-like crystals. Yield: 1.22 g (92%). ^{1}H NMR ($CDCl_3$, peaks were assigned with help of ^{1}H−^{1}H COSY experiments), δ: 2.37 (s, 3H, Me, **6**), 2.42 (s, 3H, Me, **6′**), 5.75 (s, 1H, CHNN, **6′**), 6.72 (s, 1H, OH, **6**), 7.22 (s, 1H, C_6H_4, **6′**), 7.24 (s, 1H, C_6H_4, **6′**), 7.26 (s, overlapped with the solvent signal, C_6H_4, **6**), 7.28 (s, 1H, C_6H_4, **6**), 7.36−7.48 (m, 8H, Ph, **6** + **6′**), 7.58−7.63 (m, 2H, *o*-Ph, **6**), 7.72−7.77 (m, 3H, C_6H_4 + NH, **6** + **6′**), 7.78−7.82 (m, 2H, C_6H_4, **6′**), 8.53 (s, 1H, CHNO, **6′**), 8.55 (s, 1H, CHNOH, **6**), 9.03 (s, 1H, CHNN, **6**) ppm. ^{13}C NMR spectrum is not available due to poor solubility. Anal. Calc. for $C_{16}H_{15}N_3O$ (265.31) (%): C 72.43, H 5.70 and N 15.84; found: C 72.31, H 5.63 and N 15.78.

Synthesis of 7. The precursor **2** was prepared as above. To its solution in CH_2Cl_2 (60 mL) acetone (30 mL) was added. The mixture was refluxed for 5 min. The resulting solution was left for slow evaporation and pale yellow rod like X-ray suitable crystals were formed during the next 15 min. Crystals were filtered off, washed with *n*-hexane (3 × 30 mL), and air-dried. Yield: 3.01 g (74%). ^{1}H NMR (DMSO-d_6), peaks were assigned with help of ^{1}H−^{1}H COSY experiments), δ: 1.38 (s, 60H, Me, 7′), 1.95 (s, 3H, 7), 2.07 (s, 3H, 7), 7.29−7.46 (m, 33H, *m*-Ph + *p*-Ph, 7′ + 7), 7.67−7.79 (m, 22H, *o*-Ph, 7′ + 7), 7.90 (s, 10H, CHN, 7′), 8.39 (s, 1H, CHN, 7), 8.88 (s, 10H, NH, 7′), 12.02 (br. s, 1H, OH, 7) ppm. ^{13}C NMR spectrum is not available due to poor solubility. Anal. Calc. for $C_{11}H_{13}N_3O$ (203.24) (%): C 65.01, H 6.45 and N 20.67; found: C 65.13, H 6.51 and N 20.58.

Single-Crystal X-ray Diffraction. X-ray data collection was performed on a Mar345 image plate detector using Mo K_α radiation (Xenocs Fox3D mirror) at 150(2) K for **2**, **3**, and **4′**, and 297(2) K for **5**, **6**, and **7′**. The data were integrated with the CrysAlis(Pro) software.[34] The implemented empirical absorption correction was applied. The structures were solved by direct methods using the SHELXS or SHELXT program[48] and refined by full-matrix least-squares on $|F^2|$ using SHELXL-2014.[48] Non-hydrogen atoms were anisotropically refined and the hydrogen atoms were placed at calculated positions in riding mode with temperature factors fixed at 1.2 times U_{eq} of the parent atoms and 1.5 times U_{eq} for methyl groups. Figures were generated using the program Mercury.[49]

Crystal Data for 2. $C_8H_9N_3O$, M_r = 163.18 g mol^{-1}, monoclinic, space group $P2_1/n$, a = 11.9213(6), b = 4.6621(2), c = 15.1386(7) Å, β = 104.387(5)°, V = 814.99(7) Å^3, Z = 4, ρ = 1.330 g cm^{-3}, μ(Mo−Kα) = 0.093 mm^{-1}, reflections: 5808 collected, 1493 unique, R_{int} = 0.042, R_1(all) = 0.0572, wR_2(all) = 0.1310.

Crystal Data for 3. $C_{14}H_{10}N_4$, M_r = 234.26 g mol^{-1}, orthorhombic, space group $Pca2_1$, a = 30.257(2), b = 6.1188(4), c = 18.0108(13) Å, V = 3334.5(4) Å^3, Z = 12, ρ = 1.400 g cm^{-3}, μ(Mo−Kα) = 0.088 mm^{-1}, reflections: 12667 collected, 4000 unique, R_{int} = 0.100, R_1(all) = 0.2690, wR_2(all) = 0.4573.

DOI: 10.1021/acs.joc.6b02821
J. Org. Chem. 2017, 82, 1666−1675

Crystal Data for 4′. $C_{14}H_{12}N_4O$, M_r = 252.28 g mol^{-1}, monoclinic, space group *Pn*, a = 5.8539(6), b = 27.248(2), c = 15.506(3) Å, β = 100.049(13)°, V = 2435.4(6) Å^3, Z = 8, ρ = 1.376 g cm^{-3}, μ(Mo−Kα) = 0.092 mm^{-1}, reflections: 15681 collected, 8139 unique, R_{int} = 0.059, R_1(all) = 0.1194, wR_2(all) = 0.1698.

Crystal Data for 5. $C_{15}H_{13}N_3O_2$, M_r = 267.28 g mol^{-1}, orthorhombic, space group *Pna*2$_1$, a = 13.9167(3), b = 14.5107(3), c = 6.79621(18) Å, V = 1372.43(5) Å^3, Z = 4, ρ = 1.294 g cm^{-3}, μ(Mo−Kα) = 0.089 mm^{-1}, reflections: 10403 collected, 2459 unique, R_{int} = 0.021, R_1(all) = 0.0431, wR_2(all) = 0.1131.

Crystal Data for 6. $C_{16}H_{15}N_3O$, M_r = 265.31 g mol^{-1}, monoclinic, space group *P*2$_1$/*c*, a = 13.9058(9), b = 15.9471(7), c = 14.5652(12) Å, β = 115.575(9)°, V = 2913.5(4) Å^3, Z = 8, ρ = 1.210 g cm^{-3}, μ(Mo−Kα) = 0.078 mm^{-1}, reflections: 23436 collected, 5218 unique, R_{int} = 0.040, R_1(all) = 0.0714, wR_2(all) = 0.1371.

Crystal Data for 7′. $C_{11}H_{13}N_3O$, M_r = 203.24 g mol^{-1}, monoclinic, space group *P*2$_1$, a = 5.9648(3), b = 34.2029(15), c = 10.1737(6) Å, β = 91.052(5)°, V = 2075.22(18) Å^3, Z = 8, ρ = 1.301 g cm^{-3}, μ(Mo−Kα) = 0.087 mm^{-1}, reflections: 10586 collected, 6849 unique, R_{int} = 0.024, R_1(all) = 0.0690, wR_2(all) = 0.1579.

■ ASSOCIATED CONTENT

Supporting Information

The Supporting Information is available free of charge on the ACS Publications website at DOI: 10.1021/acs.joc.6b02821.

^{1}H NMR spectra (Figures S1−S6), thermal ellipsoid plots of the crystal structures (Figures S7−S12), computational data (Figures S13−S19, S27, and S28 and Table S11), selected bond lengths and angles of the crystal structures (Tables S1−S7), Hirshfeld surface analysis and results of the charge and energy decomposition calculations (ETS-NOCV) (Figures S20−S26 and Tables S8−S10), and coordinates and absolute energies (PDF)

X-ray crystallographic data for **2** (CIF)

X-ray crystallographic data for **3** (CIF)

X-ray crystallographic data for **4′** (CIF)

X-ray crystallographic data for **5** (CIF)

X-ray crystallographic data for **6** (CIF)

X-ray crystallographic data for **7′** (CIF)

Animation of compound **5** (MPG)

Animation of compound **4-int** (MPG)

Animation of compound **4-int**···**4-int** dimer (MPG)

Animation of compound **4′** (MPG)

Animation of compound **4** (MPG)

■ AUTHOR INFORMATION

Corresponding Authors

*E-mail: damir.a.safin@gmail.com (D. A. Safin).

*E-mail: mitoraj@chemia.uj.edu.pl (M. P. Mitoraj).

ORCID

Damir A. Safin: 0000-0002-9080-7072

Mariusz P. Mitoraj: 0000-0001-5359-9107

Notes

The authors declare no competing financial interest.

■ ACKNOWLEDGMENTS

We thank WBI (Belgium) for postdoctoral positions allocated to M.G. Babashkina and D.A. Safin. DFT calculations were performed using the PL-Grid Infrastructure and resources provided by the ACC Cyfronet AGH (Cracow, Poland). We also acknowledge Fonds National de la Recherche Scientifique (FNRS, Belgium) for financial support.

■ REFERENCES

(1) Dondoni, A.; Franco, S.; Junquera, F.; Merchan, F. L.; Merino, P.; Tejero, T. *Synth. Commun.* **1994**, *24*, 2537.

(2) Franco, S.; Merchan, F. L.; Merino, P.; Tejero, T. *Synth. Commun.* **1995**, *25*, 2275.

(3) Murahashi, S. I.; Mitsui, H.; Shiota, T.; Tsuda, T.; Watanabe, S. *J. Org. Chem.* **1990**, *55*, 1736.

(4) Murahashi, S. I. *Angew. Chem., Int. Ed. Engl.* **1995**, *34*, 2443.

(5) Smith, L. I. *Chem. Rev.* **1938**, *23*, 193.

(6) Hamer, J.; Macaluso, A. *Chem. Rev.* **1964**, *64*, 473.

(7) Breuer, E. Nitrones and nitronic acid derivatives: an update. In *Nitrones, Nitronates and Nitroxides*; Patai, S., Rappoport, Z., Eds.; John Wiley & Sons: New York, 1989; Supplement U2, Chapter 3, pp 245−312.

(8) Brown, R. C. N-Oxides and Nitrones. In *Organic Chemistry of Aliphatic Compounds*; Oxford Clarendon Press: Oxford, 1994, Vol. *28*, pp 260−276.

(9) Anderson, L. L. *Asian J. Org. Chem.* **2016**, *5*, 9.

(10) Gothelf, K. V.; Jørgensen, K. A. *Chem. Rev.* **1998**, *98*, 863.

(11) Rück-Braun, K.; Freysoldt, T. H. E.; Wierschem, F. *Chem. Soc. Rev.* **2005**, *34*, 507.

(12) Kissane, M.; Maguire, A. R. *Chem. Soc. Rev.* **2010**, *39*, 845.

(13) Janzen, E. G. *Acc. Chem. Res.* **1971**, *4*, 31.

(14) Janzen, E. G.; Hiare, D. L. In *Advances in Free Radical Chemistry*; JAI Press: Greenwich, 1990; Vol. *1*, pp 253−295.

(15) Zhang, H.; Joseph, J.; Vasquez-Vivar, J.; Karoui, H.; Nsanzumuhire, C.; Martasek, P.; Tordo, P.; Kalyanaraman, B. *FEBS Lett.* **2000**, *473*, 58.

(16) Villamena, F. A.; Xia, S.; Merle, J. K.; Lauricella, R.; Tuccio, B.; Hadad, C. M.; Zweier, J. L. *J. Am. Chem. Soc.* **2007**, *129*, 8177.

(17) Floyd, R. A. *Aging Cell* **2006**, *5*, 51.

(18) Slemmer, J. E.; Shacka, J. J.; Sweeney, M.; Weber, J. T. *Curr. Med. Chem.* **2008**, *15*, 404.

(19) Piperno, A.; Giofre, S. V.; Iannazzo, D.; Romeo, R.; Romeo, G.; Chiacchio, U.; Rescifina, A.; Piotrowska, D. G. *J. Org. Chem.* **2010**, *75*, 2798.

(20) Grigorev, I. A. Nitrones: Novel Strategies in Synthesis. In *Nitrile Oxides, Nitrones, and Nitronates in Organic Synthesis: Novel Strategies in Synthesis*, 2nd ed.; Feuer, H., Ed.: John Wiley & Sons: NJ, 2008; pp 129−435.

(21) Exner, O. *J. Phys. Org. Chem.* **1990**, *3*, 190.

(22) Komaromi, I.; Tronchet, J. M. J. *J. Mol. Struct.: THEOCHEM* **1996**, *366*, 147.

(23) Huisgen, R. *Angew. Chem., Int. Ed. Engl.* **1963**, *2*, 565.

(24) Black, D. S. C.; Crozier, R. F.; Davis, V. C. *Synthesis* **1975**, *1975*, 205.

(25) Padwa, A. *Angew. Chem., Int. Ed. Engl.* **1976**, *15*, 123.

(26) Oppolzer, W. *Angew. Chem., Int. Ed. Engl.* **1977**, *16*, 10.

(27) Padwa, A. Intermolecular 1,3-Dipolar Cycloadditions. In *Comprehensive Organic Synthesis*; Trost, B. M., Fleming, I., Eds.; Pergamon Press: Oxford, 1991; Vol. *4*, pp 1069−1109.

(28) Wade, P. A. Intramolecular 1,3-Dipolar Cycloadditions. In *Comprehensive Organic Synthesis*; Trost, B. M., Fleming, I., Eds.; Pergamon Press: Oxford, 1991; Vol. *4*, pp 1111−1168.

(29) Dell, C. P. *J. Chem. Soc., Perkin Trans. 1* **1998**, 3873.

(30) Safin, D. A.; Mitoraj, M. P.; Robeyns, K.; Filinchuk, Y.; Vande Velde, C. M. L. *Dalton Trans.* **2015**, *44*, 16824.

(31) Kozhevnikov, V. N.; Kozhevnikov, D. N.; Shabunina, O. V.; Rusinov, V. L.; Chupakhin, O. N. *Tetrahedron Lett.* **2005**, *46*, 1791.

DOI: 10.1021/acs.joc.6b02821
J. Org. Chem. 2017, 82, 1666−1675

(32) Kozhevnikov, D. N.; Shabunina, O. V.; Kopchuk, D. S.; Slepukhin, P. A.; Kozhevnikov, V. N. *Tetrahedron Lett.* **2006**, *47*, 7025.
(33) Kozhevnikov, D. N.; Rusinov, V. L.; Chupakhin, O. N. In *Adv. Heterocycl. Chem.*; Katritzky, A. R., Ed.; Academic, 2002; Vol. *82*, pp 261−305.
(34) Rigaku Oxford Diffraction, *CrysAlis(Pro) Software system*, version 1.171.37.31, Rigaku Corporation: Oxford, UK, 2014.
(35) Boeyens, J. C. A. *J. Cryst. Mol. Struct.* **1978**, *8*, 317.
(36) Spackman, M. A.; Jayatilaka, D. *CrystEngComm* **2009**, *11*, 19.
(37) Grimme, S.; Antony, J.; Ehrlich, S.; Krieg, H. *J. Chem. Phys.* **2010**, *132*, 154104.
(38) Frisch, M. J.; Trucks, G. W.; Schlegel, H. B.; Scuseria, G. E.; Robb, M. A.; Cheeseman, J. R.; Scalmani, G.; Barone, V.; Mennucci, B.; Petersson, G. A.; Nakatsuji, H.; Caricato, M.; Li, X.; Hratchian, H. P.; Izmaylov, A. F.; Bloino, J.; Zheng, G.; Sonnenberg, J. L.; Hada, M.; Ehara, M.; Toyota, K.; Fukuda, R.; Hasegawa, J.; Ishida, M.; Nakajima, T.; Honda, Y.; Kitao, O.; Nakai, H.; Vreven, T.; Montgomery, Jr., J. A.; Peralta, J. E.; Ogliaro, F.; Bearpark, M.; Heyd, J. J.; Brothers, E.; Kudin, K. N.; Staroverov, V. N.; Kobayashi, R.; Normand, J.; Raghavachari, K.; Rendell, A.; Burant, J. C.; Iyengar, S. S.; Tomasi, J.; Cossi, M.; Rega, N.; Millam, J. M.; Klene, M.; Knox, J. E.; Cross, J. B.; Bakken, V.; Adamo, C.; Jaramillo, J.; Gomperts, R.; Stratmann, R. E.; Yazyev, O.; Austin, A. J.; Cammi, R.; Pomelli, C.; Ochterski, J. W.; Martin, R. L.; Morokuma, K.; Zakrzewski, V. G.; Voth, G. A.; Salvador, P.; Dannenberg, J. J.; Dapprich, S.; Daniels, A. D.; Farkas, Ö.; Foresman, J. B.; Ortiz, J. V.; Cioslowski, J.; Fox, D. J. *Gaussian 09*, Revision D.01; Gaussian Inc.: Wallingford CT, 2009.
(39) Johnson, E. R.; Keinan, S.; Mori-Sánchez, P.; Contreras-García, J.; Cohen, A. J.; Yang, W. *J. Am. Chem. Soc.* **2010**, *132*, 6498.
(40) Contreras-García, J.; Johnson, E. R.; Keinan, S.; Chaudret, R.; Piquemal, J. P.; Beratan, D.; Yang, W. *J. Chem. Theory Comput.* **2011**, *7*, 625.
(41) Michalak, A.; DeKock, R. L.; Ziegler, T. *J. Phys. Chem. A* **2008**, *112*, 7256.
(42) Vande Vondele, J.; Hutter, J. *J. Chem. Phys.* **2003**, *118*, 4365.
(43) Krack, M.; Parrinello, M. *NIC Series*; Forschungszentrum Jülich, 2004; Vol. *25*, p 29.
(44) Vande Vondele, J.; Krack, M.; Mohamed, F.; Parrinello, M.; Chassaing, T.; Hutter, J. *Comput. Phys. Commun.* **2005**, *167*, 103.
(45) Roca-López, D.; Darù, A.; Tejero, T.; Merino, P. *RSC Adv.* **2016**, *6*, 22161.
(46) te Velde, G.; Bickelhaupt, F. M.; Baerends, E. J.; Fonseca Guerra, C.; van Gisbergen, S. J. A.; Snijders, J. G.; Ziegler, T. *J. Comput. Chem.* **2001**, *22*, 931 and references therein..
(47) Baerends, E. J.; Autschbach, J.; Bashford, D.; Bérces, A.; Bickelhaupt, F. M.; Bo, C.; Boerrigter, P. M.; Cavallo, L.; Chong, D. P.; Deng, L.; Dickson, R. M.; Ellis, D. E.; van Faassen, M.; Fan, L.; Fischer, T. H.; Fonseca Guerra, C.; Ghysels, A.; Giammona, A.; van Gisbergen, S. J. A.; Götz, A. W.; Groeneveld, J. A.; Gritsenko, O. V.; Grüning, M.; Harris, F. E.; van den Hoek, P.; Jacob, C. R.; Jacobsen, H.; Jensen, L.; van Kessel, G.; Kootstra, F.; Krykunov, M. V.; van Lenthe, E.; McCormack, D. A.; Michalak, A.; Mitoraj, M.; Neugebauer, J.; Nicu, V. P.; Noodleman, L.; Osinga, V. P.; Patchkovskii, S.; Philipsen, P. H. T.; Post, D.; Pye, C. C.; Ravenek, W.; Rodríguez, J. I.; Ros, P.; Schipper, P. R. T.; Schreckenbach, G.; Seth, M.; Snijders, J. G.; Solà, M.; Swart, M.; Swerhone, D.; te Velde, G.; Vernooijs, P.; Versluis, L.; Visscher, L.; Visser, O.; Wang, F.; Wesolowski, T. A.; van Wezenbeek, E. M.; Wiesenekker, G.; Wolff, S. K.; Woo, T. K.; Yakovlev, A. L.; Ziegler, T. *ADF2012.01, Theoretical Chemistry*; Vrije Universiteit, Amsterdam.
(48) Sheldrick, G. M. *Acta Crystallogr.* **2015**, *C71*, 3.
(49) Bruno, I. J.; Cole, J. C.; Edgington, P. R.; Kessler, M.; Macrae, C. F.; McCabe, P.; Pearson, J.; Taylor, R. *Acta Crystallogr., Sect. B: Struct. Sci.* **2002**, *58*, 389.

DOI: 10.1021/acs.joc.6b02821
J. Org. Chem. 2017, 82, 1666−1675